VOL. 13, NO. 11, JUNE 2018 ISSN 1819-6608
ARPN Journal of Engineering and Applied Sciences

www.arpnjournals.com

PERSISTENT PHOTOCONDUCTIVITY AND TRANSPORT PROPERTIES OF THE AIR-INDUCED SURFACE CONDUCTING DIAMOND

Fadhlia Zafarina Zakaria
Department of Physics, School of Fundamental Sciences, Universiti Malaysia Terengganu, Kuala Terengganu, Malaysia
E-Mail: fadhlia@umt.edu.my

ABSTRACT

To our knowledge this paper presents the first study on the persistent photoconductivity behaviour of hydrogen-terminated type-IIa diamond in the presence of a surface conductivity, particularly in exploring the effect of temperature. Photoconductivity measurements were performed in vacuum over a range of sample temperatures, and with a variety of photo excitation sources of varying wavelength in addition to the transport measurements on the van der Pauw devices. From the determination of the hole sheet density, the position of the Fermi energy level, with respect to the valence band maximum was determined to be between -0.18 eV and -0.22 eV. The trap states that are responsible for photo-excitation in the diamond bandgapis within about 2.4 eV of the valence band maximum. It is found that there was no significant difference in the levels of excited photocurrent for devices with optically exposed and shielded metal contacts, confirming that the photo-effects observed arise in the diamond. Our interpretation suggests an evolution from a slowly decaying process dominated by the photoexcitation and spatial separation of electrons in the near-surface regime at high temperature to a faster decay process dominated by charge trapping by boron acceptors in the bulk at low temperature. Temperature dependent transport measurements showed that our samples became more resistive, with a concurrent decrease in measured hole sheet density, as the temperature was reduced, consistent with carrier freeze out at low temperatures due to a degree of surface disorder that has been reported extensively for all but the highest quality hydrogenated diamond surfaces.

Keywords: surface conducting diamond, persistent photoconductivity, wavelength dependence, temperature dependence.

1. INTRODUCTION

Hydrogen termination of the type IIa diamond surface will result in a negative electron affinity and a lower ionization potential [1]. The originally insulating surface will turn to be conducting upon air exposure via surface transfer doping [2]. When the H-terminated surface naturally adsorbs a water layer as a result of the air exposure, the electrons from the valence band of diamond are triggered to move into the empty electronic states afforded by the red/ox couples of atmospheric molecules dissolved within the aqueous layer, resulting in accumulated holes to be restricted to the near-surface region by an upward band bending potential [3] to produce a p-type surface conductivity.

The device applications of surface conducting diamond have been explored in the fabrication of field-effect transistors (FET), chemical and biological sensors [4]. Lately, the surface conducting diamond has also been found to be a promising material for spintronic devices [5]. To date, the investigation of the photoelectrical properties of the H-terminated diamond surface has not been reported. However, we have recently reported a preliminary study of the persistent photoconductivity observed on the air-induced and fluorofullerene-induced surface conducting diamond [6]. Persistent photoconductivity, PPC is a retained conductivity observed especially in a semiconductor after the termination of light excitation [7-9]. In this study, the PPC on the surface conducting diamond is investigated to identify the defect states and to gain insight into the mechanism and the cause of PPC in the type IIa diamond following hydrogenation and air exposure. The PPC which encountered in various semiconductors including diamond has been attributed to the surface barriers [7], impurity atoms [8] or various defects which is known to degenerate the electronic properties [10]. Although diamond has been chosen as a well suited material for photon and radiation detectors [11-13] due to its strong radiation resilience and numerous special electronic properties, PPC was found to restrict the performance of these photo detectors [9, 14]. An efficient approach to study the optoelectronic properties of diamond is by measuring the temperature dependence of photoconductivity decay [8]. However, a comprehensive study of the effect of temperature on the photoconductivity of surface conducting diamond is yet to be reported.

In this work, we investigate the photoelectrical behaviour of H:C(100) by looking into the photocurrent buildups and decays as a function of time at various temperatures using a light emitting diode (LED) as the source of light excitation and at various wavelengths using various laser sources. This paper presents a study of the optoelectronic properties of surface conducting diamond and may be useful to enhance the performance of diamond-based optoelectronic devices that could give a significant contribution to the nanoelectronic and nanoscience fields. On a more practical level, it aims to provide insight into the fact that a range of achievable hole sheet densities are recorded in the laboratory for samples measured in different environments and levels of light exposure.

Prior to undertaking the systematic photoconductivity measurements as a function of temperature, using the Hall probe system, a Janis continuous flow cryostat with optical access was utilised to perform preliminary photoconductivity measurements at room temperature with a variety of laser sources. To gain more understanding of the photocurrent growth and decay

on the van der Pauw devices, conductivity measurements were similarly conducted on the devices as a function of temperature to determine the transport properties such as the hole sheet density and sheet resistance in the dark followed by under the LED excitation.

2. EXPERIMENTAL DETAILS

2.1. Materials and Procedures

The synthetic diamonds used in this study are the intrinsic single crystal (100) diamonds (IIa) with 4.5 mm × 4.5 mm dimension purchased from Element Six. Prior to hydrogen termination, the diamond samples were acid boiled in $H_2SO_4/HCLO_4/HNO_3$ solution at 1:1:1 ratio for 15 minutes to remove metallic contamination and non-carbon phase. Following the acid boil, the diamonds are rinsed in isopropanol followed by de-ionized water to remove the acid residue. The samples were then H-terminated using a high-power microwave hydrogen plasma operating at 750 W, with hydrogen pressure of 50 Torr and approximately 750˚C sample temperature for 10 minutes. Following plasma exposure, samples were allowed to cool in vacuum to room temperature. This method produces atomically smooth hydrogenated diamond surfaces with the characteristic 2x1 reconstruction and a surface roughness of typically 1 nm as determined by STM.

2.2. Wavelength dependence photoconductivity measurements

The hydrogen-terminated diamond sample with surface conductivity induced via air exposure was used for this study. Two contacts were made using copper wires which were connected onto diagonal corners of the diamond by applying silver paint. The H-terminated diamond sample was affixed to a Si sample holder using vacuum grease and then mounted onto the sample stage of the continuous-flow cryostat with optical access through a vacuum window. This sample is referred as Sample A. Photoconductivity measurements were obtained using a variety of laser sources of different wavelengths. Besides green laser of 532 nm in wavelengths, other laser sources used for excitation were a tunableHeNe laser producing red light (632.8 nm) and an Ar ion laser for blue light (457 nm and 488 nm).

In all cases the sample was left in dark conditions for three hours prior to illumination and each laser was subsequently switched on for 60s with the same operating power of 2mW. Prior to, during and following laser exposure, the current across the sample was measured as a function of time using a Keithleypicoammeter with a bias of 1V applied using a DC power supply. The measurements were performed at a vacuum pressure of $2x10^{-6}$ mbar and at temperature of 294K. In the case of the green laser, two different experimental conditions were measured; after leaving the sample in dark condition for 3 hours and after leaving it in the dark overnight.

2.3. Temperature dependent Van der Pauw resistivity measurements

Four metal contacts of Ti/Pt/Au (50, 50, 100 nm) layers are evaporated in a Van der Pauw arrangement at the corners of the H-terminated diamond. Prior to evaporation the diamond was masked with Tantalum foil to shield from evaporating the areas outside the contact regions. The wire bonds were contacted to the van der Pauw contacts using electrically conducting silver epoxy, and wire bonded to the pins of the DIL sample holder. This Van der Pauw device is referred as Device B, was mounted into our standard ceramic DIL chip carrier and loaded into the DIL sample holder of the Hall probe.

The configuration of van der Pauw measurements was controlled with a dedicated Matlab code and the Keithley Switch System was used to undertake the set of measurements. In each orientation a current of +/-10 µA was applied to the sample. All configurations were measured in the dark followed by under LED illumination; in each case two sheet resistances, $\rho_A$and ρ_B and average sheet resistance, ρ_{AVG} were computed at each temperature. Measurements were conducted from room temperature to 150 K in case of the uncoated device B and to 245 K for the black coated devices.

For temperature dependent photoconductivity measurements, the same LED arrangement was used, with a blue LED mounted onto the DIL sample holder alongside the diamond device and positioned to maximise the exposure of the sample surface with light. The LED was powered using a Keithleypicoammeter/voltage source, operating as a voltage source with a 100 Ω resistor in series.

2.4. Temperature dependence photoconductivity measurements

In our temperature dependent photoconductivity study, measurements were carried out on device B with contacts exposed and coated in black varnish to differentiate between the effect of illumination on the surface and the contacts. Illumination of both the diamond surface and metal contacts can possibly cause a combination of photoconductivity effects in the diamond and the photovoltaic effect in the contacts. Photoconductivity measurements were performed at several temperatures in the range from room temperature to 150 K for the devices with unpainted contacts and to 250 K with painted contacts.

The blue LED setup was kept the same as in the van der Pauw measurements based on the photodiode calibration to ensure that the device was illuminated with light of constant intensity at different temperatures. Each type of device B is left in the dark for 4 hours at a particular temperature before photoconductivity measurement is carried out. Prior to running each photoconductivity measurement, the resistance of the device had been measured at each temperature. In this way, the LED is turned off and the sample is then left in dark condition to prepare for the photoconductivity measurement. Measurement at every temperature is conducted on a different day with the system heated to

room temperature prior to measurements at different temperatures.

The dark current is recorded initially followed by the photocurrent growth during the LED illumination for 15 minutes and then photocurrent decay after the illumination is terminated. All photoconductivity measurements were performed on two diagonal contacts of the H-terminated diamond in the van der Pauw geometry. A DC power supply was used to apply 2V between the contacts and a picoammeter was used to record the dark current and photocurrents.

2.5. Fitting procedure

The transient photocurrent data are fitted with a stretched exponential decay function using Origin to extract important parameters such as the decay time constant, τ and the decay exponent, β. The decay data are taken from the moment the light source was switched off in each case. Prior to fitting, the individual decay curves were normalized to unity at t=0, as shown in Figures 2 and 6. All decay curves were fitted from t=0 to t=5000 s using the fitting procedures in Origin. In this paper, all decay curves are fitted with the following stretched exponential function:

$$I(t) = I_0 e^{-\left(\frac{t}{\tau}\right)^{\beta}} + y_0 \quad (1)$$

where β is the decay exponent and τ is the decay time constant. $I(t)$ is the current at time t, and I_0 is the photocurrent directly after the LED/laser illumination was terminated, defined as t=0. The β is restricted to values between 0 and 1 which corresponds to the stretched exponential.

3. RESULTS AND DISCUSSIONS

3.1. Photoconductivity at different laser wavelengths

Figure-1 shows the photocurrent increase as a function of time during exposure at the four laser wavelengths. The constant current value for each, which corresponds to the dark current, is recorded initially prior to switching on the laser. Upon exposure, the photocurrent starts to build up until it reaches the highest photocurrent value after 60 seconds of laser exposure, at which point the excitation is terminated. It was found that the photocurrents achieved have increased by one to eight times higher than the dark current after the excitation, with higher photocurrents achieved in the case of lower laser wavelength. The maximum gain in photocurrent (after 60 s exposure time), relative to the original dark current in each case, is also plotted in Figure 1 as a function of laser wavelength. The observed dependence of the photocurrent attained on excitation wavelength shows a considerable increase in photocurrent for excitation wavelengths below 532 nm. This suggests that the observed photocurrent behaviour arises from electronic excitation for photon energies exceeding about 2.3 eV.

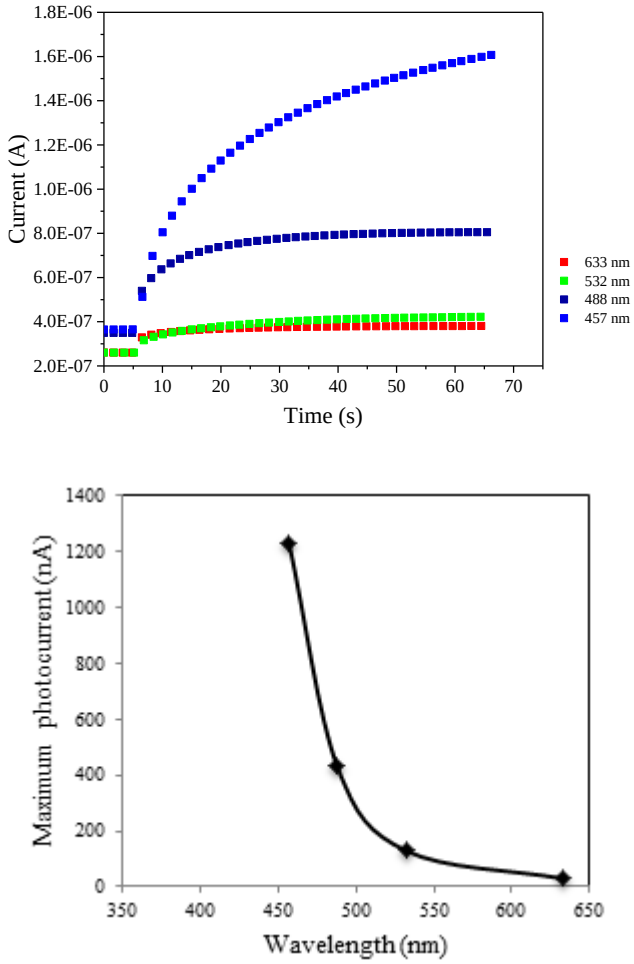

Figure-1. Current growth as a function of time of different lasers wavelengths. The lower graph illustrates the maximum gain in current after 60 s laser exposure as a function of the laser wavelength.

The origin of the excited charge is not as clear. In general, photo excitation could result from the generation of electrons in the bulk, and/or the excitation of electrons from the valence band into gap states in the near surface region giving rise to an increase in the hole density in the surface accumulation layer. Previous studies have removed the surface hole accumulation completely by studying oxygen-terminated samples in order to explore the bulk excitation of electrons [15]. In this case nitrogen-rich (type Ib) substrates were used where photo-induced currents are derived from electronic excitation of nitrogen defects. In the present case we wish to study photoconductivity in the presence of the hole accumulation layer and therefore do not have the luxury of removing the diamond bulk! Presumably, the excitation of electrons in the bulk would contribute to some extent to the photocurrents observed.

However, the levels of photocurrent observed in the present study are significantly higher than those observed by Heremans *et.al.* [15] who applied to devices electric fields of about 10^3 times higher than in our case in order to detect the photocurrent induced by bulk electrons.

VOL. 13, NO. 11, JUNE 2018 ISSN 1819-6608
ARPN Journal of Engineering and Applied Sciences

In addition, density of nitrogen defects in our type IIa substrates would be about 200 times lower than in the type Ib substrates employed by Heremans. It is therefore not unreasonable to assume that the contribution of a bulk electron photocurrent to the data in the present study would be small. Furthermore, one would expect that the bulk photocurrent should not vary significantly with the level of surface doping.

Photoexcitation would occur for electrons at the Fermi level. At the highest levels of surface doping the Fermi level sits up to 0.8 eV below the valence band edge. As the doping level is reduced the Fermi energy increases, approaching and eventually exceeding the valence band maximum [16]; under such conditions photoexcitation of electrons into gap states at a fixed wavelength would become more efficient, consistent with the higher photocurrents observed for lower excitation wavelengths. With these factors considered we can therefore be relatively confident in proposing that the photocurrent observed arises predominantly from the generation of an increased hole current in the sub-surface accumulation layer.

Figure-2 collects together the normalized photocurrent decay curves as a function of time for different laser excitation wavelengths. In the figure, an example of a fitted curve using the stretched exponential decay function is shown on the decay data that corresponds to the lowest wavelength. Figure-3 shows the plot of decay constant, derived from the fitted curves, as a function of the laser wavelength. From the fits, the decay constant, τ, was found to increase as the wavelength of the excitation light was decreased.

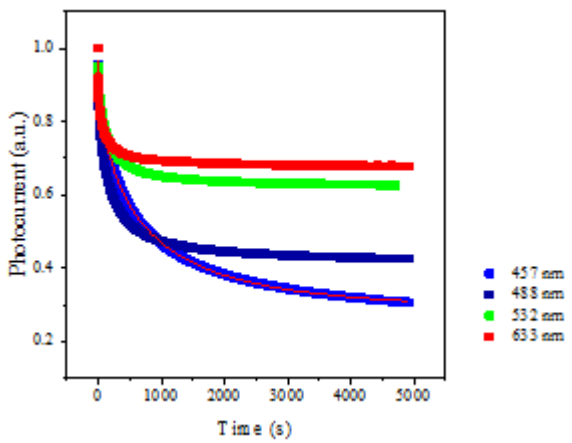

Figure-2. Normalized photocurrent decay curves after different excitation lasers at room temperature. A fitting curve using the stretched exponential function is shown at blue laser of 457 nm in wavelength.

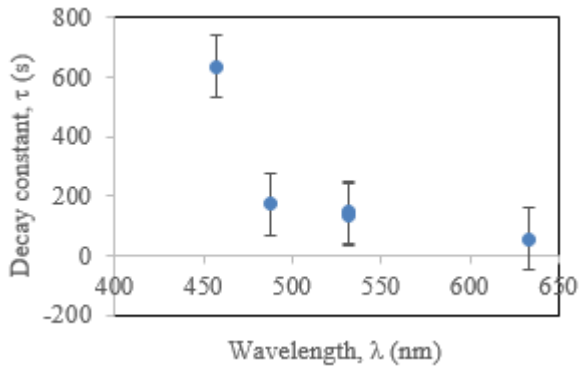

Figure-3. A plot of decay constant, τ, versus laser wavelength measured at room temperature.

The subsequent decay of the photocurrent has been explored and in all cases a persistent photocurrent, extending for several hours, was observed which could be fitted to a stretched exponential function, suggesting the role of a band or range of charge trap states. The decay time derived from the fits shows an interesting dependence on excitation wavelength, with the decay time increasing considerably as the excitation wavelength is reduced, as illustrated in Figure-3. This behaviour mirrors the data of Figure-1, showing a similar behaviour in the dependence of excitation wavelength on the attainable photocurrent, suggesting that the states responsible for the observed strong levels of photocurrent excitation at low excitation wavelength give rise to the subsequent slow decay of the photocurrent.

3.2. Temperature dependent Van der Pauw measurements

Van der Pauw measurements on the two types of device B (uncoated and black coated) were carried out to determine the conductivity of H-terminated diamond under the effect of illumination and temperature. Figure 4 shows the plot of hole sheet density, n_{2D}, with and without excitation of the blue LED, as a function of temperature. The hole density was determined from the average sheet resistance, ρ_{AVG} using a mobility, μ = 89 $cm^2V^{-1}s^{-1}$ which was determined from the Hall effect measurement on the Hall bar sample [17] that was hydrogenated under similar processing conditions. The Hall effect measurements on the Hall bar will be reported elsewhere.

In case of the device B with uncoated contacts, the sheet resistance ranges from 16.5 kΩ/□ at room temperature to 40.6 kΩ/□ at 150 K prior to LED excitation, and falls to 13.7 kΩ/□and 35.3 kΩ/□ after LED excitation for 15 minutes. For the device with painted contacts, the sheet resistance in the dark ranges from 13.5 kΩ/□to 20 kΩ/□,and from 13.0 kΩ/□ to 17.9 kΩ/□down to 245 K after the LED irradiation. The measurements on devices with unpainted and painted contacts similarly give comparable values of hole sheet density, as expected given that a fixed value of mobility is applied to determine the hole density. The measured resistance, ρ_{AVG}, was found to increase as the temperature was reduced, typical of the carrier freeze-out behaviour found for all but the best

VOL. 13, NO. 11, JUNE 2018 ISSN 1819-6608
ARPN Journal of Engineering and Applied Sciences

quality hydrogenated diamond surfaces. In accordance with ρ_{AVG} versus T, the hole density drops as temperature was decreased. Device B could only be measured reliably for temperatures down to 150 K since cooling further resulted in noisy curves.

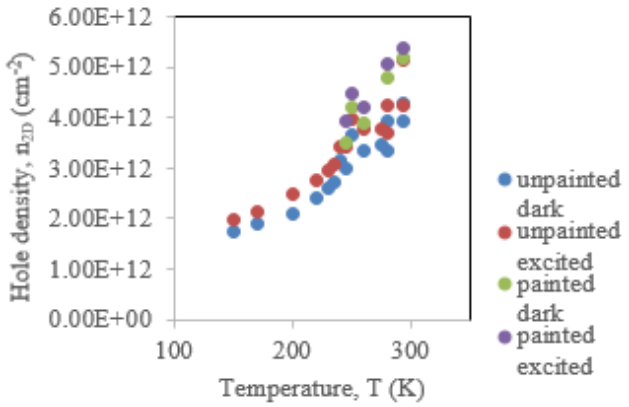

Figure-4. Hole sheet density as a function of temperature for van der Pauw devices (Device B) with unpainted and painted contacts, measured under dark conditions and with LED excitation.

After excitation, the sheet resistance decreases by 7 to 17 % and 4 to 11 % for the device with unpainted and painted contacts, respectively. The density increases by 7 to 20 % and 4 to 12 % after excitation for the unpainted and painted device, respectively. The changes in resistance and hole density as a function of temperature show that there is not a substantial difference in the response of device B to LED excitation when the contacts are bare or painted. This points towards the fact that the observed photoresponse must arise from photoconductivity effects in the diamond and not photovoltaic effects in the metal contacts. There is a trend showing that the relative increase in conductivity, represented as a percentage decrease in resistance and increase in hole density, is slightly greater as the temperature is lowered.

Using the universal relationship between E_F-E_{VBM} and hole sheet density described by Edmonds *et.al.* [16], we can estimate from our measurements of hole sheet density the position of the Fermi level with respect to the diamond valence band maximum, E_F-E_{VBM}. According to Edmonds *et al.* [16], for hole sheet densities that are higher than 10^{12} cm^{-2} the Fermi level lies below the valence band maximum, while for lower hole density values cause the Fermi level to reside above the valence band maximum, in the band gap. For the unpainted device B, the hole sheet density was determined to be between 2 $x10^{12}cm^{-2}$ at 150 K and 4 $x10^{12}$ cm^{-2} at room temperature in the dark which corresponds to E_F-E_{VBM} of between -0.18 eV at 150 K and -0.2 eV at room temperature. After a period of photoexcitation with the blue LED, the hole sheet density increased to between 2 $x10^{12}$ $cm^{-2}$and 5 $x10^{12}$ cm^{-2}which corresponds to similar values for E_F-E_{VBM}, in the range -0.18 eV to -0.22 eV.

Assuming photoexcitation in the near-surface region occurs for electrons at the Fermi level, we can therefore determine the approximate location, relative to the valence band maximum, of the gap states that are accessed via LED excitation at 2.6 eV. For a hole sheet density of 4 $x10^{12}$ cm^{-2} (at room temperature) and corresponding E_F-E_{VBM} of -0.2 eV, illumination at 2.6 eV would excite electrons into a gap state at 2.4 eV. With a reduction in temperature to 150 K, and corresponding fall in hole density to 2 $x10^{12}cm^{-2}$, E_F-E_{VBM} = -0.18 eV and the accessed gap state would be slightly higher at 2.42 eV relative to the valence band maximum. This observation may explain the trend mentioned above whereby the photoconductivity gave rise to a slightly higher relative decrease (increase) in resistance (hole density) at lower temperatures. At lower temperature, the Fermi level resides slightly closer to the valence band maximum so illumination would excite electrons to gap states that are slightly higher in energy.

3.3. Temperature dependence photoconductivity on Van der Pauw devices

The current growth is recorded from the dark condition to the moment the LED is turned on until immediately before the LED excitation is terminated. Figures 5 a) and b) show the comparison of the normalized current build ups for all temperatures. The normalisation is carried out from unity at *t*= 0s. The two types of Device B have been excited for approximately 15 minutes which is equivalent to 900s. It is shown in the figure that the higher current growth corresponds to the higher dark current which occurs at high temperatures. Lower temperatures tend to have lower dark currents and have smaller current increment after the LED is excited on the sample. The curves from the painted device resemble the unpainted data at low temperatures. The growth curves of the uncoated devices are plotted in separate graphs for clarity.

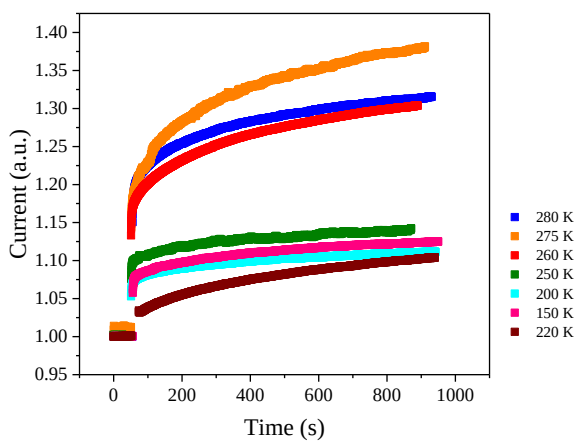

(a)

VOL. 13, NO. 11, JUNE 2018 ISSN 1819-6608
ARPN Journal of Engineering and Applied Sciences

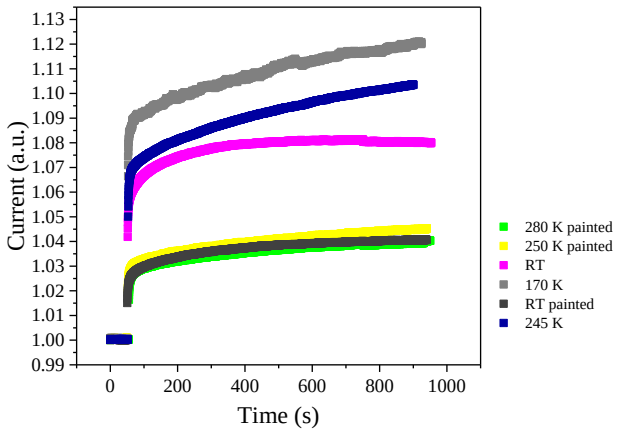

(b)

Figure-5. Normalized photocurrent growth from dark level until a point of LED de-excitation at various temperatures for (a) uncoated device only and (b) black coated device including three temperatures of the uncoated device. Note: some curves are not fully visible due to coincident with other data.

The current increment from the dark current, I_0 to the highest photocurrent immediately prior to turning off the LED for various temperatures were found to be relatively constant from 150 K to 250 K with 10 to 15 % increase from the dark current values but reaching more than 30 % at higher temperatures of between 260 to 280 K. The highest increase of 38 % corresponds to 275 K. This jump however returns to less than 8 % at room temperature in case of the unpainted device B and becomes constant again with 4 to 5 % increase between 250 K and room temperature in case of the painted or black coated device.

Normalized photocurrent decay curves at some temperatures, together with the fits, are shown in Figure-6. The fitted curves of the photocurrent decay obtained on device B with uncoated contacts were shown at RT, 280 K, 245 K and 150 K and some of the similar temperatures were shown for the corresponding black coated device for comparison. These curves are shown in separate plots for clarity. In each case the black traces are data points obtained from experiments and the red curve represents the fit to a stretched exponential. From the fitting, it is observed that most photocurrent decay curves are fitted nicely to Equation (1).

The fitted curves at room temperature, 280 K, 275 K, 260 K, 245 K, 200 K, 170 K and 150 K in case of the unpainted device are considered as good fits as the fitting curve coincides with most traces of the data points and all the three decay curves of the black coated contacts of device B at room temperature, 280 K and 250 K fit well with the stretched exponential decay function. The values of the decay constant, τ and decay exponent, β are extracted from the fitting of the subsequent photocurrent decay curves to the stretch exponential decay function. The decay exponent, β values from the curves of both devices are determined to be smaller than 0.41 for all temperatures which demonstrate a real stretching behaviour. β is related to the trapping state density and the release rates from the trapping centre [18].

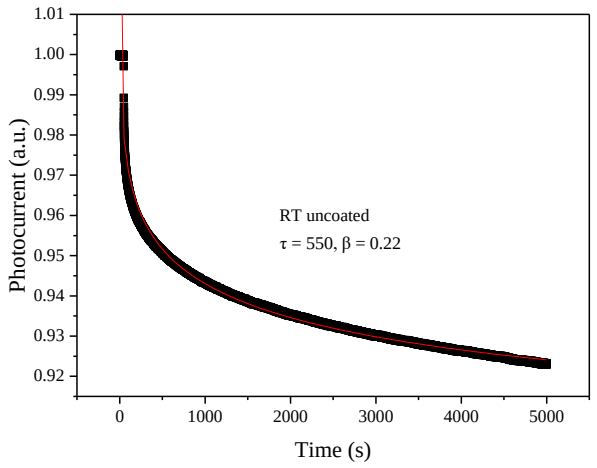

(a)

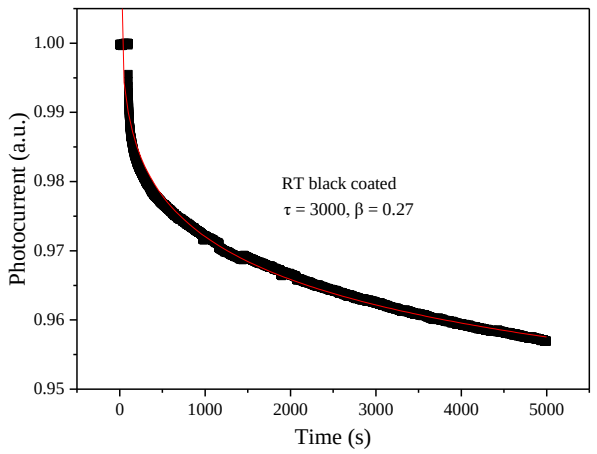

(b)

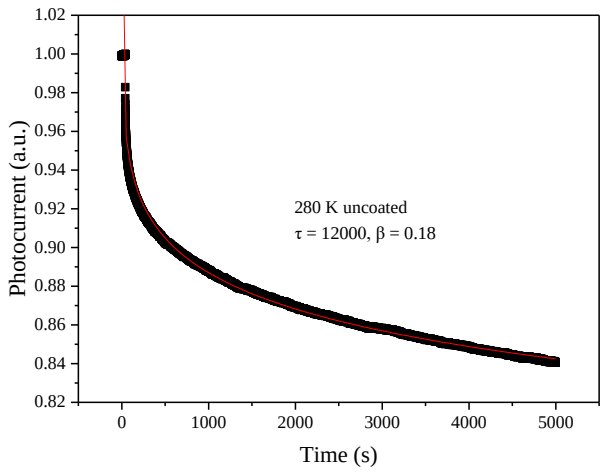

(c)

VOL. 13, NO. 11, JUNE 2018 ISSN 1819-6608
ARPN Journal of Engineering and Applied Sciences

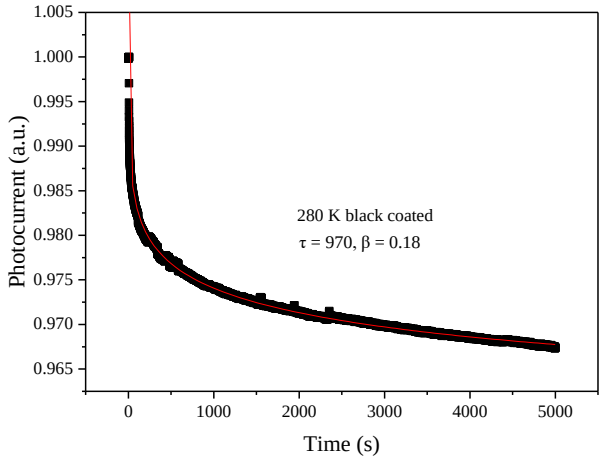

(d)

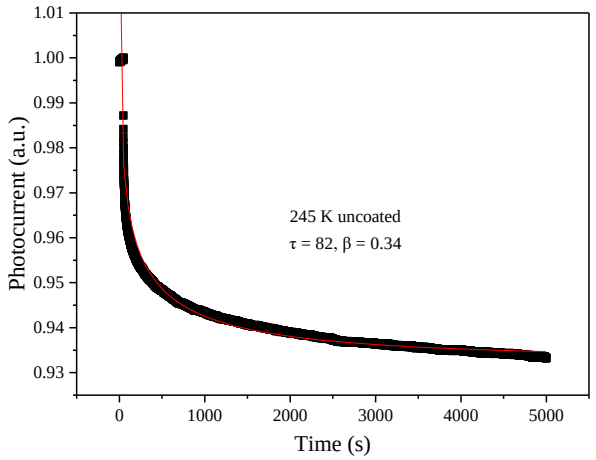

(e)

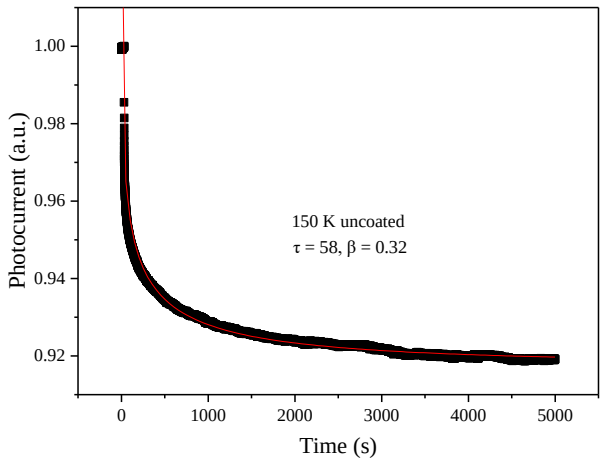

(f)

Figure-6. Normalized photocurrent decay at some temperatures for device B with uncoated contacts at (a) room temperature (c) 280 K (e) 245 K (f) 150 K; and black coated contacts at (b) room temperature (d) 280 K. The black curve is the data while the red curve represents the fit.

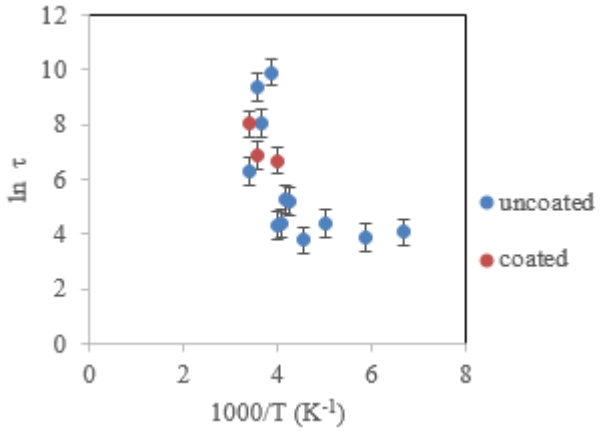

Figure-7. ln(τ) plotted as a function of 1000/T for uncoated and black coated devices from room temperature to 150 K. The coated devices were measured at three temperatures only; at RT, 280 K and 250 K.

A plot of ln(τ) versus 1000/T, derived from the fitted photocurrent decay curves, is shown in Figure-7. The error bar for τ is determined to be 0.5 at all temperatures. The observed behaviour in ln(τ) against temperature shows distinct differences when compared to persistent photocurrent decay characteristics observed in the literature. The work of Liao *et.al.* [8], probing deliberately boron-doped diamond epilayers with deep ultra-violet and white-light photoexcitation and Hang *et.al.* [19], studying InGaAs quantum wells, serve as useful reference points for comparison with the present study. In the case of Liao *et.al.* [8], a positive persistent photocurrent effect was observed in samples deliberately doped with boron concentration of 10^{16} cm^{-3} and absent in cases when the boron concentration was below 10^{15} cm^{-3}. The persistent photocurrent was ascribed to detrapping of holes from these boron acceptors in the epilayer with a resulting ln(τ) that was constant, and equal to about 5, up to a temperature of about 450 K, and decreased at higher temperatures.

As evident in Figure-7, in the present case the decay time is seen to be independent of temperature in the range 150 K to 250 K with approximately the same value, but rises steadily from 250 K to room temperature. The boron concentration in the IIa substrates used in the present study is < 0.05 ppm which, for a diamond number density of 1.7 x10^{23} cm^{-3}, amounts to a boron concentration of no greater than about 8 x10^{15} cm^{-3}. This level is at the lower limit implied by Liao *et.al.*, so it is not unreasonable to consider that boron acceptors in the diamond bulk may play a role in trapping photoexcited electrons in the present study at low temperatures.

We now turn to consider the data for temperatures greater than 250 K, for which considerably higher values of ln(τ), accompanied by smaller values of β, evolve up to room temperature. As we have shown, the hole sheet density in the sub-surface conducting layer is higher close to room temperature, as a result of carrier freeze-out at low temperature, and we earlier showed evidence that for water-doped samples the level of

photocurrent developed increased with the dark current in the surface conducting channel. It may therefore be the case that the slow decay behaviour observed in the high temperature regime arises from charge excitation and trapping with a longer decay time predominantly at the diamond surface.

The work of Hang *et. al.* [19] is of interest here since it shows over a certain temperature regime an increase in ln(τ) with temperature. The complex persistent photoconductivity behaviour observed by Hang *et.al.* [19] could not be explained by defect trapping alone and was described qualitatively by a model based upon the competition between the photo-excitation of a two-dimensional electron gas and the spatial separation of the photoexcited charge carriers into the conduction band of neighbouring barriers giving rise to slower decay rates.

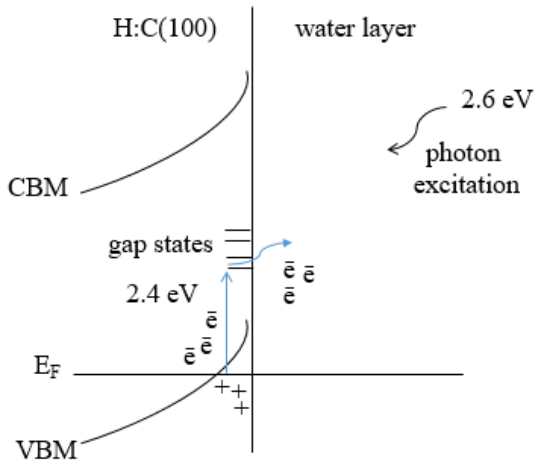

Figure-8. A schematic band diagram illustrating potential charge transfer and trapping mechanisms where charges are excited from the Fermi energy into gap states and subsequently transfer into acceptor states in the water layer.

The present scenario is considerably different to that of the InGaAs/InAlAshetero structures studied by Hang *et. al.*, but there are some similarities. For surface transfer doped diamond in the dark state, electrons transfer from the valence band of the diamond into acceptor states in an adsorbed water layer, giving rise to subsurface hole accumulation and band bending. It may be the case that in the high temperature regime of our measurements, photoexcited electrons may have sufficient thermal energy to similarly transfer into the neighbouring surface water layer with subsequent decay to recombine with holes in the diamond necessitating the transfer across the water-diamond interface. The potential charge transfer is illustrated in the schematic band diagram of Figure-8.

The photoconductivity effects that we report in this paper have not been observed for oxygen terminated diamond surface. Further studies are required to fully test the feasibility of our possible explanation for the complex observed temperature dependence in ln(τ). Our interpretation suggests an evolution from a slowly decaying process dominated by the photoexcitation and spatial separation of electrons in the near-surface regime at high temperature to a faster decay process dominated by charge trapping by boron acceptors in the bulk at low temperature.

CONCLUSIONS

The photoconductivity behaviour and the transport properties of the surface conducting diamond have been explored.

From the determination of the hole sheet density and position of the Fermi level, relative to the valence band maximum, in the dark state it is suggested that the trap states responsible for photo-excitation in the diamond bandgap is within about 2.4 eV of the valence band maximum.

We have found that there was no significant difference in the levels of excited photocurrent for devices with optically exposed and shielded metal contacts, confirming that the photo-effects observed arise in the diamond.

Systematic temperature dependent photoconductivity decay measurements indicate that the persistent photoconductivity at low temperature may arise from trapping due to boron impurities in the diamond bulk and that above 250 K the PPC is dominated by a different trapping mechanism with a longer decay process that is unrelated to the mechanism at lower temperature that gives rise to a shorter decay.

ACKNOWLEDGEMENTS

Author would like to thank Professor Chris Pakes, Golrokh Akhgar and Robert Polglase from the Department of Chemistry and Physics, School of Molecular Sciences, La Trobe University, Victoria, Australia; and Dr. Laurens Willems van Beveren, Dr. Timothy Karle, Dr. Desmond Lau and Stephen Gregory from the Department of Physics, The University of Melbourne, Australia for their assistance.

We would like to thank Dr. Julius Orwa for transporting some hardwares to the University of Melbourne for the preliminary measurements, Professor Lothar Ley for his advice on the photodiode calibration and Dr. Jiri Cervenka/ Dr. Alastair Stacey for hydrogen terminating our diamond samples. The author is grateful to Universiti Malaysia Terengganu and Malaysia's Ministry of Higher Education for the scholarship provided.

REFERENCES

[1] Ristein J. 2005. Diamond surfaces: familiar and amazing. Applied Physics A. 82 (3): 377-384.

[2] Maier F., Riedel M., Mantel B., Ristein J. and Ley L. 2000. Origin of Surface Conductivity in Diamond. Physical Review Letters. 85(16): 3472-3475.

[3] Nebel C. E., Rezek B., Shin D. and Watanabe H. 2006. Surface electronic properties of H-terminated

diamond in contact with adsorbates and electrolytes. Physica Status Solidi (a). 203(13): 3273-3298.

[4] Pakes C. I., Garrido J. A. and Kawarada H. 2014. Diamond surface conductivity: Properties, devices, and sensors. CVD Diamond-Research, Applications, and Challenges. 39(6): 542-548.

[5] Akhgar G., Creedon D. L., Willems van Beveren L. H., Stacey A., Hoxley D. I., McCallum J. C., Ley L., Hamilton A. R. and Pakes C. I. 2018. G-factor and well width variations for the two-dimensional hole gas in surface conducting diamond. Applied Physics Letters. 112(4): 042102.

[6] Fadhlia Zafarina Zakaria. 2018. Photoconductivity Effects in Air-induced and Fluorofullerene-induced Surface Conducting Diamond. ARPN Journal of Engineering and Applied Sciences. 13(5): 1918-1923.

[7] Koide Y. and Liao M. 2007. Mechanism of photoconductivity gain for p-diamond Schottky photodiode. Diamond and Related Materials. 16: 949-952.

[8] Liao M., Koide Y., Alvarez J., Imura M. and Kleider J. 2008. Persistent positive and transient absolute negative photoconductivity observed in diamond photodetectors. Physical Review B. 78(4): 045112.

[9] Wang L., Chen X., Wu G., Guo W., Cao S., Shang K. and Han W. 2011. The mechanism of persistent photoconductivity induced by minority carrier trapping effect in ultraviolet photo-detector made of polycrystalline diamond film. Thin Solid Films. 520: 752-755.

[10] Remes Z., Uzan-Saguy C., Baskin E., Kalish R., Avigal Y., Nesladek M. and Koizumi S. 2004. Photo-Hall effect measurements in P, N and B-doped diamond at low temperatures. Diamond and Related Materials. 13(4-8): 713-717.

[11] Almaviva S., Marinelli M., Milani E., Prestopino G., Tucciarone A., Verona C., Verona-Rinati G., Angelone M. and Pillon M. 2009. Extreme UV photodetectors based on CVD single crystal diamond in a p-type/intrinsic/metal configuration. Diamond and Related Materials. 18(1): 101-105.

[12] Tromson D., Bergonzo P., Brambilla A., Mer C., Foulon F. and Amosov V. N. 1999. Thermally Stimulated Investigations on Diamond Based Radiation Detectors. Physica Status Solidi (a). 174(1): 155-164.

[13] Bergonzo P. and Jackman R. B. 2004. Diamond-based radiation and photon detectors. Semiconductors and Semimetals. 77: 197-310.

[14] Remes Z., Petersen R., Haenen K., Nesladek M. and D'Olieslaeger M. 2005. Mechanism of photoconductivity in intrinsic epitaxial CVD diamond studied by photocurrent spectroscopy and photocurrent decay measurements. Diamond and Related Materials. 14: 556-560.

[15] Heremans F., Fuchs G., Wang C., Hanson R. and Awschalom D. 2009. Generation and transport of photoexcited electrons in single-crystal diamond. Applied Physics Letters. 94(15): 152102.

[16] Edmonds M., Pakes C., Mammadov S., Zhang W., Tadich A., Ristein J. and Ley L. 2011. Work function, band bending, and electron affinity in surface conducting (100) diamond. Physica Status Solidi (a). 208(9): 2062-2066.

[17] Fadhlia Zafarina Zakaria. 2017. Fabrication and Measurement of Surface Nanoelectronic Devices in Diamond. Ph.D. Thesis, La Trobe University, Victoria, Australia.

[18] Chen R. 2003. Apparent stretched-exponential Luminescence decay in crystalline solids. Journal of Luminescence. 102-103: 510-518.

[19] Hang D. R., Chen Y. F., Fang F. F. and Wang W. I. 1999. Positive and negative persistent photoconductivity in a two-side-doped $In_{0.53}Ga_{0.47}As/In_{0.52}Al_{0.48}As$ quantum well. Physical Review B. 60(19): 13318-13321.